Contrasting hydrological controls on bed properties during the acceleration of Pine Island Glacier, West Antarctica

M. Bougamont[1*] , P. Christoffersen[1] , I. Nias[2†] , D. G. Vaughan[3] , A. M. Smith[3] , A. Brisbourne[3]

(1) Scott Polar Research Institute, Univ. of Cambridge, Cambridge, UK
(2) Bristol Glaciology Centre, Univ. of Bristol, Bristol, UK
(3) British Antarctic Survey, Natural Environment Research Council, Cambridge, UK

*Corresponding author: Marion Bougamont (mb627@cam.ac.uk)
†Current address: Earth Syst. Sci. Interdisciplinary Ctr, Univ. of Maryland, College Pk, MD, USA, and Cryos. Sci. Lab., Goddard Space Flight Ctr, NASA, Greenbelt, MD, USA.

Content of this file:

This file contains Supplementary Tables S1 and S2, and Figures S1 to S6.

Table S1: Modelled basal stress and changes in basal stress in areas of *weakening*, which covers 75% of the speed-up region, using the same ice geometry for the 1996 and 2014 inversions.

	Median τ_f (kPa)	Quantiles τ_f [0.1 0.25 0.75 0.9] (kPa)	Median $\Delta\tau_f$		Quantiles $\Delta\tau_f$ [0.1 0.25 0.75 0.9] (kPa)
			kPa	%	
I_{1996_MC}	21	[8 12 50 89]			
I_{2014_MC}	17	[6 10 42 79]	-3	-16	[-11 -5.9 -1.6 -0.8]

Table S2: Modelled basal stress and changes in basal stress in areas of *strengthening,* which covers 25% of the speed-up region, using the same ice geometry for the 1996 and 2014 inversions.

	Median τ_f (kPa)	Quantiles τ_f [0.1 0.25 0.75 0.9] (kPa)	Median $\Delta\tau_f$		Quantiles $\Delta\tau_f$ [0.1 0.25 0.75 0.9] (kPa)
			kPa	%	
I_{1996_MC}	45	[12 19 88 116]			
I_{2014_MC}	53	[14 23 95 131]	3.3	9	[0.4 1.2 8.3 16.8]

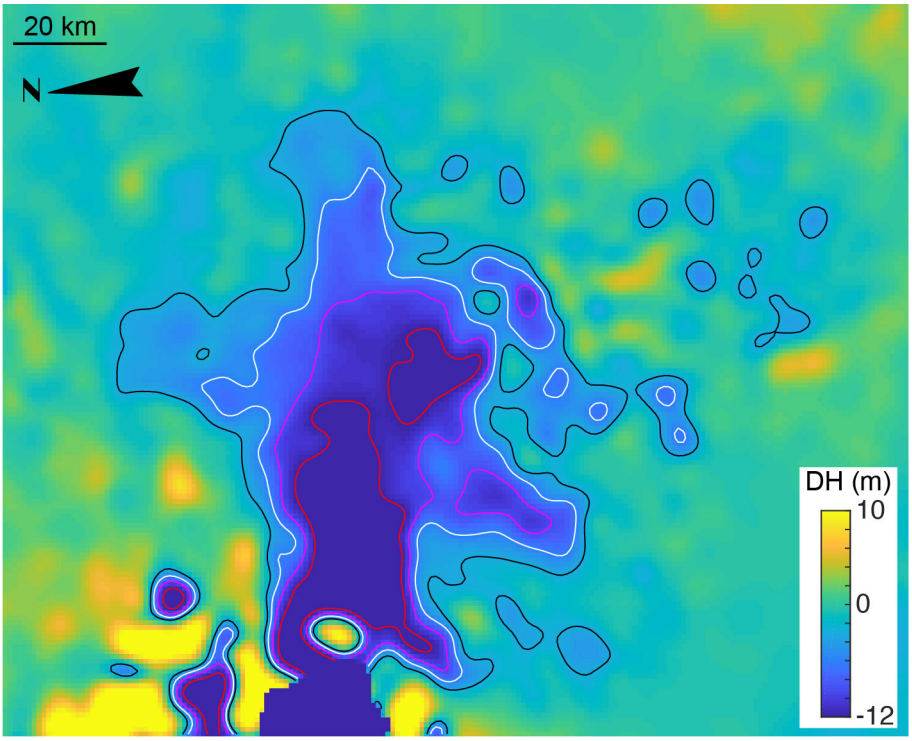

Figure S1: Surface elevation difference (m) between 1996 and 2014, obtained from calculating the difference measured between IceSat (2004-06) and Cryosat (2011-13) data. The contours value are -3 m (black), -6 m (white), -9 m (magenta) and -12 m (red).

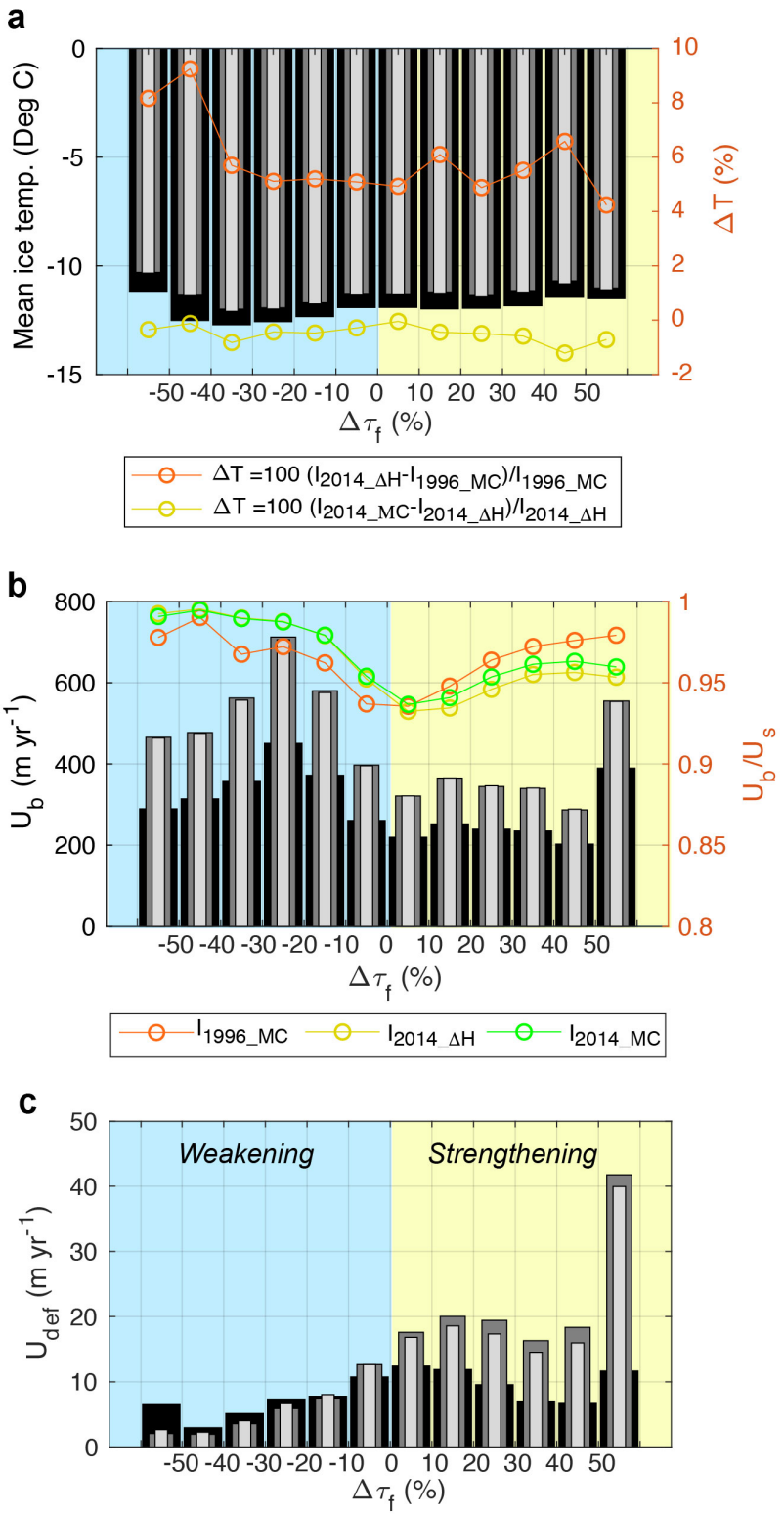

Figure S2: **Left axes:** Histogram with bins showing the average value of **(a)** ice temperature (deg C), **(b)** basal velocity (m yr^{-1}) and **(c)** deformational velocity (m yr^{-1}), where basal drag weakened (blue shade) and strengthened (yellow shade) between 1996 and 2014 (change in %, labelled on the x-axes). Results are shown for I_{1996_MC} (black bins), $I_{2014\_\Delta H}$ (dark grey bins), and I_{2014_MC} (light grey bins). **Right axes: (a)** Difference in ice temperature (%) calculated between I_{1996_MC} and $I_{2014\_\Delta H}$ (orange), and between $I_{2014\_\Delta H}$ and I_{2014_MC} (yellow). The difference between I_{1996_MC} and $I_{2014\_\Delta H}$ indicate a uniform warming of the ice in the $I_{2014\_\Delta H}$ inversion, which is due to increased heat dissipation, and reduced conductive heat losses at the ice base in response to velocity changes. The difference between $I_{2014\_\Delta H}$ and I_{2014_MC} confirms that the thinning applied in the $I_{2014\_\Delta H}$ inversion does not significantly impact the steady-state ice

temperature in 2014. **(b)** Ratio of basal velocity over surface velocity for I_{1996_MC} (orange), $I_{2014\_\Delta H}$ (yellow), and I_{2014_MC} (green), indicating that the deformational velocity is a very small component of the surface velocity everywhere in the domain.

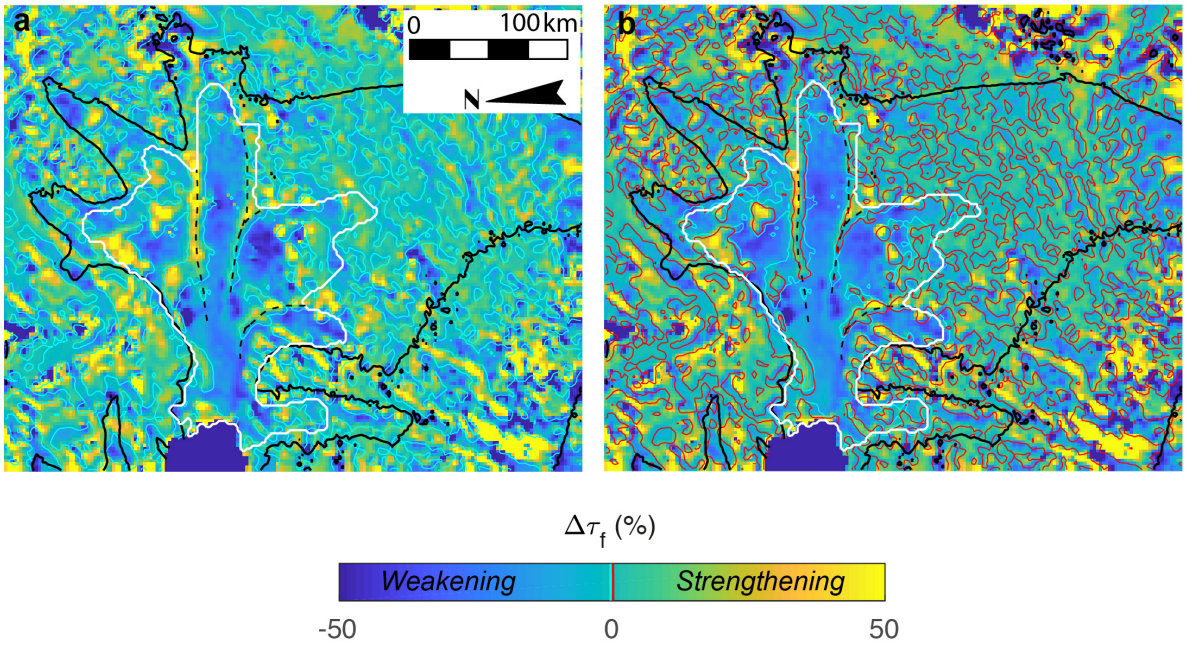

Figure S3: Sensitivity of the modelled change in basal stress to the ice geometry used for the 2014 inversion. On panels (a) and (b), the black line shows the 50 m yr^{-1} of the 2014 surface velocity contour, the white line outlines the region of significant speed-up, and the dashed black lines identify zones of sticky spots coincident with shear margin location (as in Fig. 3). **(a)** Change in basal drag (%) between inversions I_{1996_MC} and $I_{2014\_\Delta H}$. The 0-value contour for $\Delta\tau_f$ is shown in cyan. **(b)** Change in basal drag (%) between inversions I_{1996_MC} and I_{2014_MC}. The 0-value contour for $\Delta\tau_f$ is shown in red. To facilitate the comparison, we also plot the 0-value contour for $\Delta\tau_f$ shown in panel (a) (cyan).

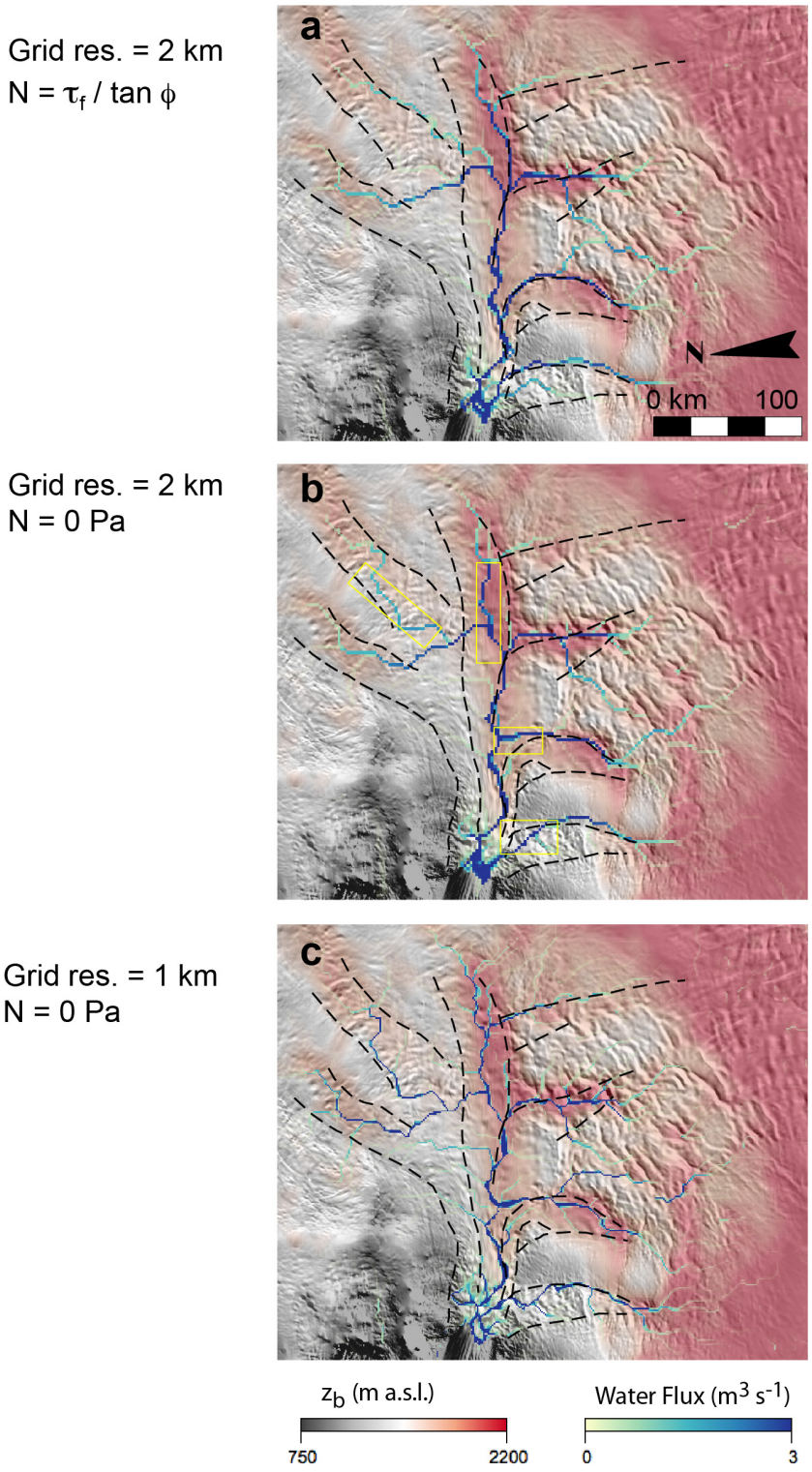

Figure S4: Sensitivity of subglacial water routing to effective pressure in the subglacial environment and to grid resolution, based on the 1996 surface velocity inversion. **(a)** Water routing presented in the main text, overlain on bed topography (m a.s.l.), and with shear margin location (dash black lines). The model grid resolution is 2 km, and the effective pressure is calculated from the till shear strength (Eq.7). **(b)** Water routing with a model grid resolution of 2 km, and assuming that the effective pressure is 0 Pa. The overall water pathways are broadly similar, with path modifications (highlighted in yellow boxes) not sufficient to impact our results interpretation. **(c)** Water routing with a grid resolution of 1 km, and assuming that the effective pressure is 0 Pa. This suggests that the water routing is not sensitive to the grid resolution used in our study.

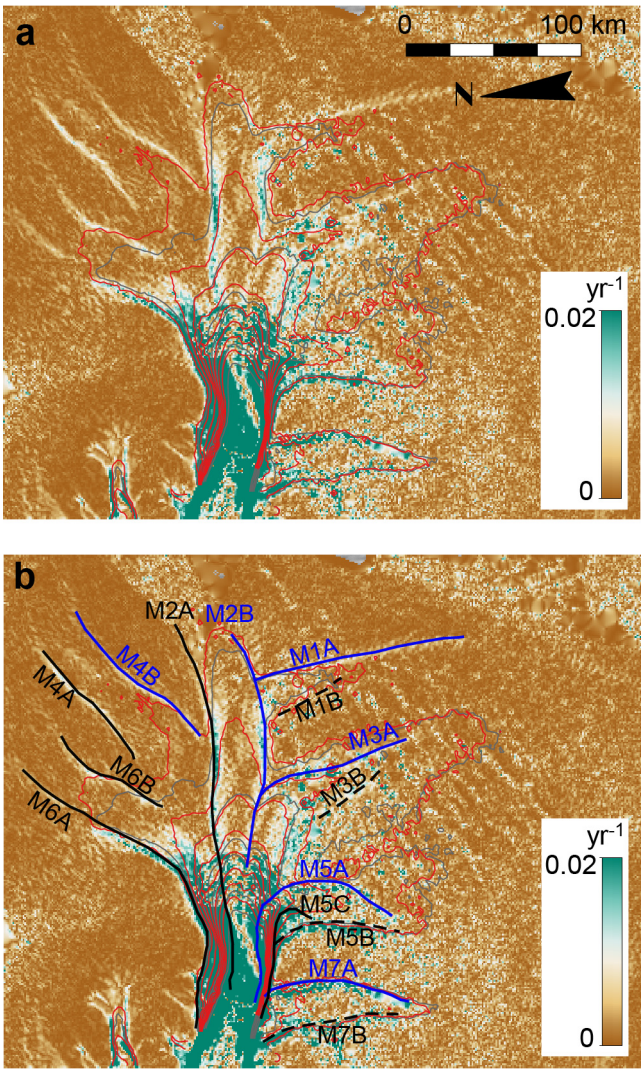

Figure S5: Maps of PIG showing **(a)** shear strain rates (yr^{-1}) calculated with the surface velocity observed in 2014, and velocity contours (200 m yr^{-1} spacing, 2014 values in red, and 1996 values in grey). **(b)** as in (a), with identified margin location used in the main text. The position of margins appears to have remained stable since 1996.

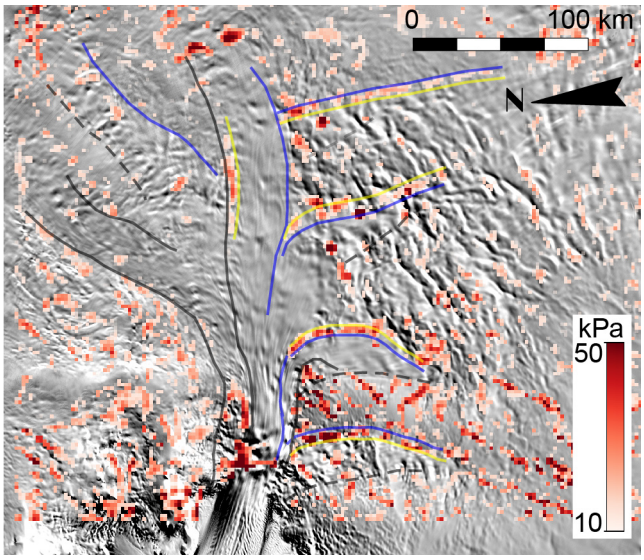

Figure S6: Map of PIG showing basal strengthening between 1996 and 2014 (kPa), highlighting values of minimum 10 kPa. Color-coded margin positions are shown as in the main text. The yellow lines identify the marginal zones where we hypothesize strong basal strengthening to be the direct result of hydrological processes.